plate are confined to a very narrow zone near the wing root. This is probably due to the presence of a strong crossflow in the inboard direction, typical of forward-swept wings, that limits the spanwise propagation of the interference effects. Therefore, one may conclude that, for these types of wings, the experimental data are affected by the interference with the splitter plate only in a limited zone close to the wing root.

Acknowledgments

The present work has been financially supported by the Ministero della Università e Ricerca Scientifica. The authors gratefully acknowledge the Council for Scientific and Industrial Research of Pretoria, South Africa, for providing the experimental results.

References

[1]Milholen, W. E., II, and Chokani, N., "Effect of Sidewall Boundary Layer on Transonic Flow over a Wing," *Journal of Aircraft*, Vol. 31, No. 4, 1994, pp. 986–988.

[2]Lombardi, G., Salvetti, M. V., and Morelli, M., "Appraisal of Numerical Methods in Predicting the Aerodynamics of Forward-Swept Wing," *Journal of Aircraft*, Vol. 35, No. 4, 1998, pp. 561–568.

[3]Lombardi, G., "Experimental Aerodynamic Effects of a Forward Sweep Angle," *Journal of Aircraft*, Vol. 30, No. 5, 1993, pp. 629–635.

[4]Buresti, G., Lombardi, G., and Morelli, M., "Pressure Measurements on Different Canard-Wing Configurations in Subsonic Compressible Flow," Atti Del Dipartimento Di Ing. Aerospaziale Di Pisa, Rept. ADIA 91-4, Pisa, Italy, Sept. 1991.

[5]*RAMPANT User's Guide*, Release 4.0, Fluent, Lebanon, NH, April 1996.

Spreadsheet Fluid Dynamics

Etsuo Morishita*
University of Tokyo,
Hongo, Bunkyo-ku, Tokyo 113-8656, Japan

Nomenclature

Gr = Grashof number
Nu = Nusselt number
P = excess pressure
Pr = Prandtl number
p = static pressure
Ra = Rayleigh number ($=PrGr$)
Re = Reynolds number
T = temperature
t = time
u, v = velocity components
x, y = coordinates
ζ = vorticity
ψ = stream function

Introduction

COMPUTATIONAL fluid dynamics (CFD) is one of the most important branches of fluid dynamics. CFD enables a detailed analysis of flowfields, which otherwise is very difficult. In the learning stage of CFD, however, many researchers have had problems in regard to code development for scientific and engineering calculations, not only because of the complexity of the governing equations but also because of computer programming rules. This still often is the case among younger students who are just beginning to study numerical simulations.

Received 5 January 1998; revision received 10 February 1999; accepted for publication 22 February 1999.

*Professor, Department of Aeronautics and Astronautics, Graduate School of Engineering. Senior Member AIAA.

Currently available personal computer software, however, might enable us to do scientific computing without developing lengthy computer programs, depending on the situation. In particular, spreadsheet software is widely used at home and also for scientific calculations.[1] We realize that spreadsheets are extremely valuable for fluid dynamics simulations, as well as for other simulations.[2] The cells in the spreadsheet can be viewed as natural grids for computation and their assigned function can be iterated upon. Spreadsheets usually include graphics software and therefore the computational results can be visualized easily. When the spreadsheet is used for fluid dynamics calculations, we need the differential form of the governing equations and the boundary conditions. First, we define the computational domain in a spreadsheet. Typically, a steady two-dimensional fluid dynamics problem is assumed, e.g., a rectangular computational domain is selected. The boundary condition then is written in a cell on the boundary. This can be copied to other cells by copy-and-paste procedures. Before we write the boundary conditions, boundary cells should be colored, thereby making it easy to recognize the computational domain. Then, we write the governing equations in one of the cells in the computational domain. We copy the cell contents to other cells into the computational domain again by using spreadsheet copy-and-paste commands. Next we select the circular reference[1] calculation and decide on the number of iterations and the solution error tolerance. The computation is repeated automatically and we may continue the calculation until the desired convergence is achieved. When convergence is reached, we select the computational domain and visualize the results almost instantly using the inherent graphics software.

Spreadsheet fluid dynamics (SFD) is easy to use and does not require any special knowledge about the computer language being used (it is fair to say that it is already programmed). It is also possible to visualize the results during the computation and to interactively change the computational conditions, including the form of the equations and the boundary conditions.

SFD Procedure

We use Laplace's equation to illustrate the SFD procedure. The governing equation for the stream function of a potential flow is given by

$$\nabla^2 \psi = 0 \tag{1}$$

From the finite difference form of Eq. (1) for square grids, we can obtain at (x_i, y_j):

$$\psi_{i,j} = \frac{\psi_{i+1,j} + \psi_{i-1,j} + \psi_{i,j+1} + \psi_{i,j-1}}{4} \tag{2}$$

We used Eq. (2) for the potential flow over a step, shown in Fig. 1, i.e., a spreadsheet. The cells on the boundary should be colored for clarity. We specify the boundary conditions on the boundary cells. We input the value of the stream function on the boundary. So, in Fig. 1, $\psi = 0$ is used for the cells on the lower boundary (including the step), and $\psi = 1$ is used for the cells on the upper horizontal boundary. The inlet and outlet flows may be assumed to be uniform and a linear distribution of the stream function is used, i.e., $\psi = y$.

	A	B	C	D	E	F	G	H	I	J	K	L	M
1	dx	dy											
2	0.1	0.1											
3													
4		psi											
5			1	1	1	1	1	1	1	1	1	1	1
6			0.9										0.9
7			0.8										0.8
8			0.7										0.7
9			0.6										0.6
10			0.5										0.5
11			0.4										0.4
12			0.3				0	0	0				0.3
13			0.2				0	0	0				0.2
14			0.1				0	0	0				0.1
15			0	0	0	0	0	0	0	0	0	0	0

Fig. 1 Spreadsheet for a stream function ψ for flow over a step.

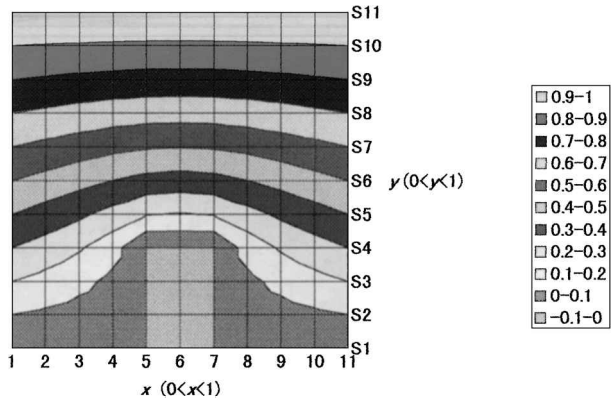

Fig. 2 Stream function ψ obtained by spreadsheet iteration and its graphics.

In the computational domain, we insert Eq. (2) into all internal cells. We chose cell D6 in Fig. 1 and the finite difference equation (2) is expressed by the spreadsheet format as follows[1]:

$$= (E6 + C6 + D5 + D7)/4 \tag{3}$$

Equation (3) then is copied onto other cells in the computational domain and the relative references[1] work accordingly by automatically changing the symbols in Eq. (3).

We then use the circular reference calculation function.[1] We can specify the number of iterations and the maximum function changes.[1] While the spreadsheet undergoes the iteration procedure, we can interrupt the calculation and check the result either by the numbers in the cell or a graph that shows the stream function.

The final result for Fig. 1 is shown in Fig. 2. The maximum change (error tolerance) that we selected for the stream function was 10^{-9}, and the same value also was used for the rest of the physical values in the present calculations. The graphics software that we incorporated is readily available and an almost instantaneous numerical flow visualization is possible. Note that we only need one spreadsheet to specify the boundary conditions, describe and solve the governing equations, and visualize the calculated results. Velocity and pressure fields also can be obtained easily from the stream function.

Some Typical Problems Solved by SFD

Inlet Channel Flow and Temperature Field

We first studied an incompressible steady inlet flow of a two-dimensional channel and its temperature field. The governing equations in nondimensional forms are[3]

Continuity:

$$\frac{\partial u}{\partial x} + \frac{\partial v}{\partial y} = 0 \tag{4}$$

Momentum:

$$\frac{\partial u}{\partial t} + u\frac{\partial u}{\partial x} + v\frac{\partial u}{\partial y} = -\frac{\partial p}{\partial x} + \frac{1}{Re}\nabla^2 u \tag{5}$$

$$\frac{\partial v}{\partial t} + u\frac{\partial v}{\partial x} + v\frac{\partial v}{\partial y} = -\frac{\partial p}{\partial y} + \frac{1}{Re}\nabla^2 v \tag{6}$$

Energy:

$$\frac{\partial T}{\partial t} + u\frac{\partial T}{\partial x} + v\frac{\partial T}{\partial y} = \frac{1}{PrRe}\nabla^2 T \tag{7}$$

We used the vorticity–stream function formulation[3] and Eqs. (4–6) become

$$\nabla^2 \psi = -\varsigma \tag{8}$$

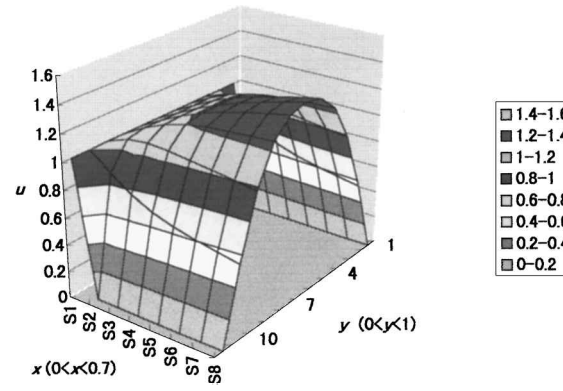

Fig. 3 Inlet velocity distribution u at $Re = 0.5 \times 10^2$.

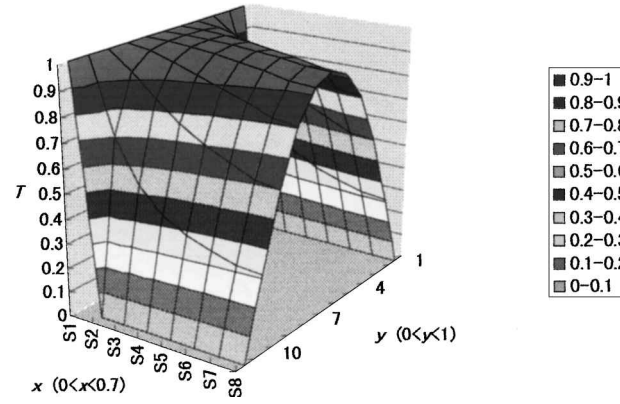

Fig. 4 Inlet temperature distribution T at $Re = 0.5 \times 10^2$ and $Pr = 0.72$.

$$\frac{\partial \varsigma}{\partial t} + u\frac{\partial \varsigma}{\partial x} + v\frac{\partial \varsigma}{\partial y} = \frac{1}{Re}\nabla^2 \varsigma \tag{9}$$

$$\nabla^2 p = 2\left(\frac{\partial u}{\partial x}\frac{\partial v}{\partial y} - \frac{\partial u}{\partial y}\frac{\partial v}{\partial x}\right) \tag{10}$$

The finite difference forms of the governing equations are obtained by the forward time/central space method.[3] The boundary conditions are given in a manner similar to those of the conventional vorticity–stream function method.[3] The uniform inlet and wall temperatures are specified.

The inlet flow calculations at $Re = 0.5 \times 10^2$ and $Pr = 0.72$ are shown in Figs. 3 and 4. The computational domain is $0 \le x \le 0.7$ (flow direction) and $0 \le y \le 1$, with $dx = dy = 0.1$ and $dt = 0.01$. Therefore 8×11 cells (grids) were used altogether. The computational domains are marked in a spreadsheet for ψ, ς, u, v, p, and T.

The development from a uniform to a parabolic velocity distribution is shown clearly in Fig. 3. The effects of the Reynolds number were checked quickly by changing its value in a cell.

The temperature development is shown in Fig. 4. $Pr = 0.72$ (air) was used in our calculations. It is clear that the temperature distribution develops because of the heat transfer on the wall.

To examine the validity of the computational results, comparisons were made with the results of Ref. 4. Figure 5 shows a comparison of the maximum velocity u_m in flow direction at midchannel, as obtained by SFD and the laminar flow analysis in the inlet section of a channel.[4] The results are fairly satisfactory, considering the coarseness of the cells that were used in computation. It was also checked that the velocity distribution by SFD approached that of the Hagen–Poiseuille flow (parabola).

Rayleigh–Benard Instability

A fluid that is between two parallel plates forms two-dimensional vortex cells when the fluid is heated from below due to the gravitational force, i.e., the buoyancy. The nondimensional governing

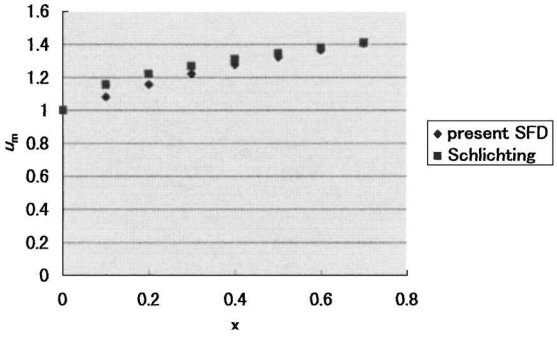

Fig. 5 Inlet u_m by SFD and laminar flow analysis[4] at $Re = 0.5 \times 10^2$.

equations for a two-dimensional example using the Boussinesq approximation are[5]

Continuity:

$$\frac{\partial u}{\partial x} + \frac{\partial v}{\partial y} = 0 \tag{11}$$

Momentum:

$$-\frac{\partial P}{\partial x} + \frac{1}{Re}\nabla^2 u = 0 \tag{12}$$

$$-\frac{\partial P}{\partial y} + \frac{1}{Re}\nabla^2 v + \frac{Gr}{Re^2}(T - T_r) = 0 \tag{13}$$

Energy:

$$u\frac{\partial T}{\partial x} + v\frac{\partial T}{\partial y} = \frac{1}{PrRe}\nabla^2 T \tag{14}$$

where the inertia forces of the fluid were neglected because we studied the phenomena around the marginal stability.[5] The vorticity–stream function formulation of Eqs. (11–13) are

$$\nabla^2 \psi = -\varsigma \tag{15}$$

$$\nabla^2 \varsigma = -\frac{Gr}{Re}\frac{\partial T}{\partial x} \tag{16}$$

$$\nabla^2 P = \frac{Gr}{Re^2}\frac{\partial (T - T_r)}{\partial y} \tag{17}$$

The discretized forms of the governing equations are obtained as Eq. (2) (Ref. 3). The boundary conditions are the same as those in the Benard cell in an enclosed space.[5,6] The initial (also reference T_r and side wall) temperature distribution is

$$T(x, y) = 1 - y \quad (=T_r) \tag{18}$$

We used characteristic velocity $U = \nu/L$ ($L =$ channel height, $\nu =$ kinetic viscosity) simply to nondimensionalize the governing equations and, therefore, the Reynolds number becomes the unity in this definition. It is also possible to use $U = \alpha/L$ ($\alpha =$ thermal diffusivity); a different definition for the characteristic velocity is $U = (\nu/L)\sqrt{Gr}$ for $\sqrt{Gr} > 1$ and $Pr < 1$ (Ref. 6).

After the velocity field was calculated, we first integrated the momentum equations (12) and (13) along the surface of the wall by assuming that the reference excess pressure is zero at the center on the bottom wall. We then used Eq. (17) to calculate the excess pressure distribution between the two parallel walls.

The computational domain was $0 \le x \le 3.2$, $0 \le y \le 1$ and 6×17 cells were used for the calculations with $dx = dy = 0.2$. The computational results for the Benard cells at $Ra = 1800$ for a rectangular area with an aspect ratio of 3.2 are shown in Figs. 6–8.

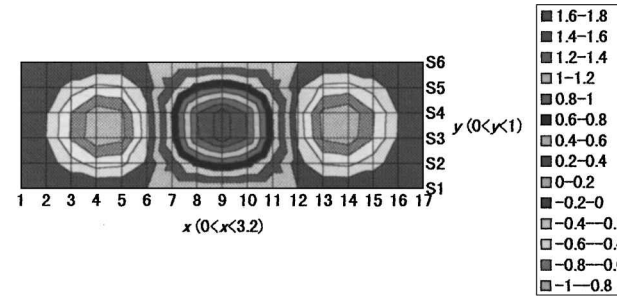

Fig. 6 Benard cell stream function ψ at $Ra = 1800$.

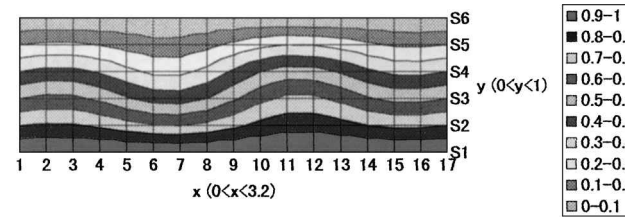

Fig. 7 Benard cell temperature T at $Ra = 1800$.

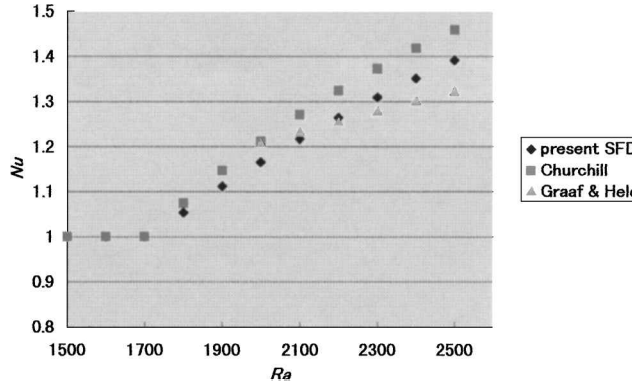

Fig. 8 Benard cell heat transfer comparison.

Figure 6 shows the stream function and it represents the Benard vortex cells between the two parallel plates; three rolling cells were visualized. The directions of the rotation were clockwise, counterclockwise, and clockwise from the left. The calculated cell aspect ratio is approximately one.

The corresponding wavy temperature distribution is shown in Fig. 7. The wavy temperature distribution suddenly appeared when the Rayleigh number exceeded a critical value at around 1700. The theoretical critical value Ra_c is 1708 for an enclosed region.[5] We started the calculation at $Ra = 1500$ and increased Ra by 100 repeatedly to $Ra = 2500$. We just have a linear stable temperature distribution at $Ra = 1700$, but we have a wavy temperature distribution at $Ra = 1800$, as is shown in Fig. 7. It is known that the temperature gradient in the x-direction exhibits a cell-like pattern.[5] The temperature gradient was obtained numerically in the spreadsheet, and three roll cells also were observed.

The vorticity has a peak value at around the center of the cells, and also has large values on the bottom and top walls. The vorticity on the side walls is not strong. We can identify the direction of the vortex cell rotation from u and v. The distribution of excess pressure P also was obtained. The large pressure gradient regions in the y-direction correspond to the cell boundary where the flow moves vertically.

The average heat transfer rate was obtained on the bottom and the top walls, and they are exactly equal in our calculations. Nu ($=-\partial T/\partial y_{\text{wall}}$) around the marginal stability is shown in Fig. 8 and was compared to the experimental correlation.[7,8] We used a first-order finite difference formula for the Nusselt number in Fig. 7.

The agreement is good, but the calculated value was 5% lower than that for Churchill's experimental correlation at $Ra = 2500$ (Ref. 7). The difference at a larger Rayleigh number can be attributed to the coarse cells and the first-order finite difference formula. We also calculated the Nusselt number by the second-order finite difference formula, and the heat transfer was estimated to be 14% higher at $Ra = 2500$ than for Churchill's experimental correlation.[7] This also can be attributed to the coarseness of the cells in the y-direction. The convection term is not included in our calculations but this effect may be small around the marginal stability. However, when we take the coarseness of the cells, the results in Fig. 8 satisfactorily show the usefulness of SFD.

Conclusions

We show that the function of the spreadsheet can be extended to CFD by using the iteration function and the circular reference. The present results demonstrate that the cells of the spreadsheet can be used as natural grids for CFD; in addition, we were able to see the computational domain during calculation by coloring the boundary cells.

SFD requires discretized governing equations and boundary conditions and these are reproduced in each cell in a spreadsheet by the copy-and-paste procedure. We then begin iteration and the computation is completed by SFD solution reaching either the specified number of iterations or the specified maximum error tolerance. The procedure was demonstrated for the potential flow over a step using Laplace's equation.

The SFD technique was extended to an inlet flow in a two-dimensional channel, where the Navier–Stokes equations were solved by the spreadsheet and the temperature field also was calculated. The results were compared with those from the laminar inlet flow calculation in order to examine the validity and the usefulness of the method.

The present SFD technique also was applied to a natural convection problem, i.e., to the Rayleigh–Benard instability. The detailed flow and temperature pattern of the Benard cell in an enclosed space with an aspect ratio of 3.2 between two parallel plates were reproduced by means of the spreadsheet computation. The heat transfer estimation was also satisfactory at $Ra = 2500$ (about 5% difference) as compared to the existing experimental correlation.

Although spreadsheets are used widely in science and engineering, this paper represents the first application for CFD equations. The computational domain is variable in spreadsheets and the practical engineering, i.e., aeronautical and mechanical, problems can be handled. Our SFD technique has the following features: 1) no prior knowledge of the computer language, 2) no program lines (e.g., Fortran coding), 3) built-in cells (grids), 4) visible computational domain during problem setup as well as computation, 5) interactive computation, and 6) computational results easily presented using the inherent graphics software.

References

[1]Walkenbach, J., "Creating and Using Formulas," *Excel 97 Bible*, IDG Books, Foster City, CA, 1996, pp. 171–237.

[2]Misner, C., and Cooney, P., "Two-Dimensional Motion," *Spreadsheet Physics*, Addison–Wesley, Reading, MA, 1991, pp. 43–56.

[3]Hoffmann, K. A., and Chiang, S. T., "Incompressible Navier–Stokes Equations," *Computational Fluid Dynamics for Engineers*, Vol. 1, Engineering Education System, Wichita, KS, 1995, pp. 288–343.

[4]Schlichting, H., "Part B Laminar Boundary Layers," *Boundary-Layer Theory*, McGraw–Hill, New York, 1979, pp. 127–448.

[5]Faber, T. E., "Instabilities," *Fluid Dynamics for Physicists*, Cambridge Univ. Press, Cambridge, England, UK, 1995, pp. 289–342.

[6]Antar, B. N., and Nuotio-Antar, V. S., "Scale Analysis in Buoyancy-Driven Convection," *Fundamentals of Low Gravity Fluid Dynamics and Heat Transfer*, CRC Press, Boca Raton, FL, 1993, pp. 136–139.

[7]Hsu, S. T., "Free Convection in an Enclosed Space Between Two Parallel Surfaces," *Engineering Heat Transfer*, Van Nostrand, Princeton, NJ, 1963, pp. 386–396.

[8]Churchill, S. W., *Heat Exchanger Design Handbook*, Springer–Verlag, Heidelberg, Germany, 1983, Sec. 2.5.8.

In-Flight Skin Friction Measurements Using Oil Film Interferometry

Aaron Drake*
Washington State University, Tri-Cities, Richland, Washington 99352-1643
and
Robert A. Kennelly Jr.†
NASA Ames Research Center, Moffett Field, California 94035-1000

Introduction

OIL film interferometry for quantitative skin friction measurement has been demonstrated successfully on an aircraft in-flight. Measurements were made during two flights of a Beech F33C Bonanza single-engine light aircraft at several locations on the wing upper surface and the flaps. Oil film interferometry is a direct skin friction measuring method first developed during the 1970s.[1–4] Transparent oil placed on a surface exposed to the airstream is thinned by the shear stress acting on it. In the original version of the technique, this thinning was measured by observation of the interference resulting from laser light reflecting from the air–oil interface and the oil–surface interface. The rate at which this thinning occurs can be related to the skin friction shear stress using lubrication theory.

The method makes use of readily available plastic sheets for optical surfaces and conventional illumination.[5–7] With several simplifying assumptions, only a single, postflight photograph of the interference pattern is required. The interference fringes can be viewed directly to obtain qualitative information or measured to obtain quantitative values of local skin friction. This technique has been demonstrated in low-speed, transonic, and supersonic wind tunnels,[5–8] but not on an aircraft in-flight.

A key assumption of this simplified method is that the skin friction coefficient ($C_{f\infty}$, defined as the local shear stress normalized by the freestream dynamic pressure) remains constant during the entire time the oil is exposed to the flow. Although this requirement is met easily in wind tunnels (perhaps only approximately in transonic and supersonic wind tunnels), the possibility of developing a flight profile with sufficiently brief takeoff and landing, off-condition, segments to satisfy this assumption remained unknown.

Procedure

Measurements were made during two flights. Adhesive-backed Mylar sheets (Monokote™, Top Flite Models, Inc., Champaign, IL) were placed on the surface to provide suitable optical properties to permit visible interference fringes. The locations are shown in Fig. 1. A line of transparent oil, in this case dimethylpolysiloxane (Dow–Corning, Midland, Michigan), was placed on the Mylar just before flight. For the first flight, oil with a nominal viscosity of 200 cS was used; for the second, higher-speed flight, a 500-cS formulation was used.

Lines of oil were applied just before flight. There were approximately 30 oil lines, most applied perpendicular to the freestream flow direction. Three oil lines also were placed at approximately 45 deg to the wing's leading edge. These lines, covering the upstream 30% chord of the wing at approximately midsemispan, were for the detection of boundary-layer transition. Because of the large

Received 7 October 1997; revision received 9 February 1999; accepted for publication 9 February 1999.

*Ph.D. Candidate, Department of Mechanical Engineering; currently Senior Engineer, Raytheon Aircraft Co., Wichita, KS 67201. Member AIAA.

†Aerospace Engineer, High-Speed Aerodynamics Branch. Senior Member AIAA.